  Bull. Chem. Soc. Jpn., 55, 1003—1013 (1982)

Thermodynamic Study of NH_4Br and ND_4Br Crystals under Constant High-pressures†

Kazuo WATANABE,** Masaharu OGUNI, Takasuke MATSUO, Hiroshi SUGA,* and Syûzô SEKI***

Department of Chemistry and Chemical Thermodynamics Laboratory, Faculty of Science, Osaka University, Toyonaka, Osaka 560

(Received October 26, 1981)

Heat capacities and volumes of NH_4Br and ND_4Br crystals were measured in the temperature range from 100 to 260 K at several constant pressures up to 110 MPa with a special attention paid to the behaviors around the point of ND_4Br at 66 MPa and 202 K. The experimental results at an atmospheric pressure were in good agreement with the previously reported ones. The δ-γ and δ-β phase transitions were accompanied with expansion of the volume while the γ-β phase transition with contraction. Detailed phase diagram obtained for ND_4Br disclosed that there was no maximum in any branch of the transition lines. The triple point was represented essentially as the point of intersection of the three straight lines. There was no pressure dependence of the total entropy of transition from the δ to β phase. The entropy values can be explained by the mechanism of the order-disorder change in the orientations of NH_4^+ tetrahedra. The existence of the heat capacity anomaly in the high temperature side of the δ-γ phase transition was discussed as due to the spatial fluctuation of domains of the γ and δ phases. An argument was put forward that the observed δ-γ phase transition was probably superheated. An additional anomalous heat-capacity peak was observed just below the triple point pressure in between the temperatures of the δ-γ and γ-β phase transitions, and explained in terms of the effects of the superheating in the δ-γ phase transition and of the coexistence of the δ and γ phases domains in the crystal.

There have been four phases known to exist in the NH_4Br crystal at the atmospheric pressure.[1] They are named α through δ phases in the order of the high to low temperature in respect of the temperature range of their occurrence. As the pressure increases, the temperature range of the stability of the γ phase becomes small and disappears at the triple point pressure of 160 MPa for NH_4Br and 66 MPa for ND_4Br.[1,2]

These phases are distinguished from one another by the differences in the interrelation of orientations of NH_4^+ ions and in the relative positions of the ions.[3] The α phase has the NaCl structure in which NH_4^+ ions are orientationally disordered. The β phase has the CsCl structure with the NH_4^+ ions in the state of disorder between two different orientations in the octahedral crystal field. The structure of the γ phase is in the tetragonal system; adjacent NH_4^+ ions take a parallel orientation along the c axis and an anti-parallel one within the ab plane, and the Br^- ions accordingly shift themselves slightly along the c-axis with concomitant shortening of the N–H···Br hydrogen bonds. The δ phase has the same cubic structure as the β phase, but with NH_4^+ ions in the parallel ordered state in the orientations.

Two different mechanisms, order-disorder in configurational degrees of freedom and displacement of atoms and ions away from the high symmetry sites, are in general considered as basic atomic processes of phase transitions in ionic crystals. In the transitions among the β, γ, and δ phases there are two competing ordering interactions.[4] A direct octupole-octupole interaction between nearest-neighbor NH_4^+ tetrahedra energetically favors a parallel ordering realized in the δ phase, while an indirect interaction of the tetrahedra through the polarizable Br^- ions stabilizes the anti-parallel ordering accompanied by the displacement of the Br^- ions in the γ phase.

We reported construction of an adiabatic calorimeter working under constant high pressures.[5] In the present paper we report calorimetric and volumetric studies of the phase transitions in NH_4Br and ND_4Br crystals performed with this apparatus with special attention paid to the behavior around the triple point of ND_4Br. In general the behavior of a substance around the triple point involving the gaseous, liquid, crystalline phases is determined only by the difference in the magnitudes of the free energies for these phases. The γ-β and δ-β phase transitions in the present crystals have been well known from various experimental techniques to be of the λ type.[6–9] The behavior around such triple points as associated with phase lines of the λ type was expected to be different from that of the gas-liquid-crystal triple points on account of the continuous interrelation among the crystal structures involved.

Experimental

Materials. Crystalline ammonium bromide NH_4Br (Nakarai Chemical Co. Ltd., special reagent) was purified by sublimation at about 140 °C under vacuum. The powder sample obtained was pressed into pellets of 2 cm in diameter and 0.7 cm in thickness for closer packing in the cell. The mass of the sample used was 37.593 g corresponding to 0.38383 mol.

The sample in the calorimeter cell was pressurized through direct contact with pressure medium, 3-methylpentane, for a uniform hydrostatic pressure. This method is applicable if the sample is insoluble in the liquid. The solubility was checked with a spectroscopic method; NH_4Br was first extracted into water phase from the saturated 3-methylpentane solution, and then the ultraviolet spectra of the aqueous solution was compared with those of the aqueous NH_4Br solutions of known concentration. The amount-of-substance fraction of

† Contribution No. 27 from Chemical Thermodynamics Laboratory.

** Present address: Kanzaki Paper Mtg. Co. Ltd., 1-11, Jōkōji-Motomachi, Amagasaki 660.

*** Present address: Department of Chemistry, School of Science, Kwansei Gakuin University, Nishinomiya 662.

NH_4Br in the pressure medium was estimated to be less than 10 ppm, indicating that the above method of pressurization caused no serious problem in the heat capacity measurements.

Ammonium-d_4 bromide (ND_4Br) sample was prepared by recrystallizing the purified NH_4Br crystals from deuterium oxide (Nakarai Chemical Co. Ltd., 99.8%) solution three times. Deuterium exchange ratio of the powder sample was found by high resolution ^1H-NMR method to be 99.5%. The calorimeter cell contained 35.418 g (0.34734 mol) of the sample in pellet form. All the procedures of the preparation and handling were carried out in the atmosphere of dry nitrogen gas.

The densities of NH_4Br and ND_4Br crystals at room temperature were calculated from data of the mass and volume of the pellet. The volume was obtained by measuring the pellet sizes with a micrometer.

Calorimetric Procedures. The calorimeter cell was loaded with the sample at room temperature and screwed up at liquid nitrogen temperature for tight sealing. Setting-up of the cell in the cryostat and introduction of 3-methylpentane into the high-pressure system were carried out in the same manner as described already.[5]

A series of heat capacity measurement at several constant pressures was performed in the intermittent heating mode with the temperature step of 2—3 K. The volume of the sample at each temperature and pressure was calculated by using the compressibility and expansivity data of 3-methylpentane given in the previous paper.[5]

Results and Discussion

Heat Capacities at an Atmospheric Pressure. Heat capacity values of NH_4Br and ND_4Br crystals at an atmospheric pressure are shown in Figs. 1 and 2, respectively, together with the previously reported data obtained by using an ordinary adiabatic calorimeters.[10-12] They are in good agreement within the inaccuracy of 1% except at temperatures just around the phase transition points. In view of the adverse circumstances in determining the heat capacity values with the present calorimeter, this agreement would be satisfactory. Evidently, unfavorable factors incurred by the high pressure were overcome in the present apparatus. It is now possible to measure high-pressure heat capacities with almost the same accuracy as with the ordinary adiabatic calorimeter under the atmospheric pressure.

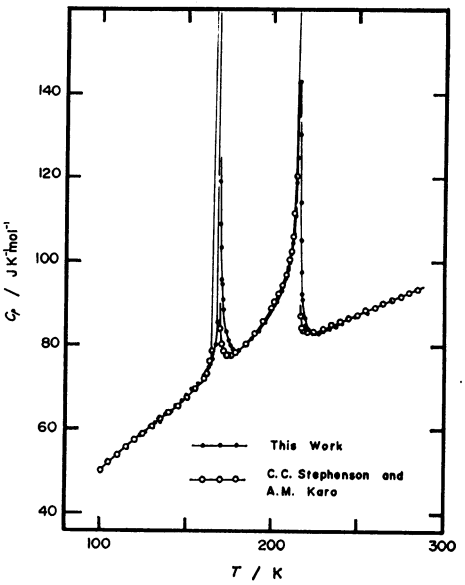

Fig. 2. Molar heat capacity of ND_4Br crystal at an atmospheric pressure.

Table 1. The entropies of the phase transitions in NH_4Br and ND_4Br crystals

Substance	Ref.	$\Delta_\alpha^\gamma S$ / J K^{-1} mol^{-1}	$\Delta_\gamma^\beta S$ / J K^{-1} mol^{-1}	$\Delta_\alpha^\beta S$ / J K^{-1} mol^{-1}
NH_4Br	10	1.1	3.0	4.1
	11	1.1	3.0	4.1
	This work	1.2	2.6	3.8
ND_4Br	12	—	—	5.4
	This work	—	—	5.0

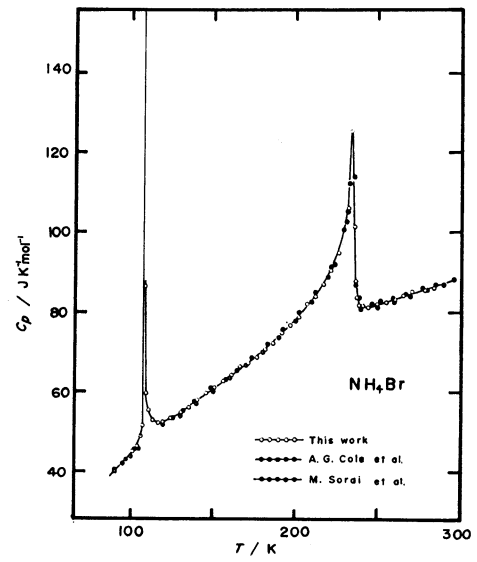

Fig. 1. Molar heat capacity of NH_4Br crystal at an atmospheric pressure.

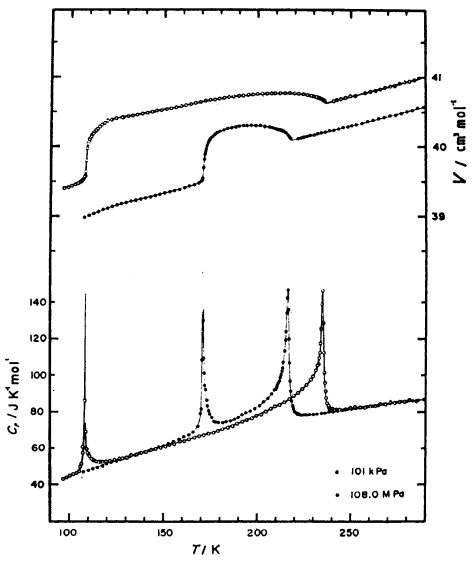

Fig. 3. Molar heat capacity and molar volume of NH_4Br at 0.101 (○) and 108.0 MPa (●).

TABLE 2. MOLAR HEAT CAPACITY AND MOLAR VOLUME OF NH_4Br

T / K	C_p / $J K^{-1} mol^{-1}$	V / $cm^3 mol^{-1}$	T / K	C_p / $J K^{-1} mol^{-1}$	V / $cm^3 mol^{-1}$	T / K	C_p / $J K^{-1} mol^{-1}$	V / $cm^3 mol^{-1}$	T / K	C_p / $J K^{-1} mol^{-1}$	V / $cm^3 mol^{-1}$
P = 101 kPa			217.02	87.04	40.770	232.08	78.70	40.179	181.69	74.03	40.231
			219.46	88.78	40.765	234.10	79.13	40.192	183.79	74.39	40.252
96.81	42.98	39.395	221.83	90.27	40.763	236.10	79.32	40.200	185.88	74.99	40.262
98.78	43.96	39.413	224.15	92.51	40.752	238.27	79.91	40.221	187.97	76.03	40.270
100.71	44.96	39.434	226.37	94.72	40.739	240.67	79.89	40.228	190.04	76.94	40.283
102.49	45.47	39.452	228.51	97.50	40.731	243.16	80.36	40.247	192.09	78.55	40.291
104.13	46.30	39.468				245.64	80.69	40.262	194.14	79.64	40.294
105.29	47.07	39.483	219.89	88.88	40.768	248.14	81.33	40.278	196.34	80.33	40.294
105.93	49.89	39.494	222.40	90.87	40.760	250.37	81.54	40.294	198.75	81.88	40.294
106.44	51.44	39.507	224.91	93.04	40.747	252.82	81.75	40.309	201.18	83.46	40.294
106.84	51.26	39.522	227.41	95.97	40.737	255.85	82.27	40.330	203.60	85.50	40.283
107.17	51.60	39.533	229.78	99.27	40.724	258.86	82.74	40.353	205.85	87.28	40.273
107.52	55.37	39.554	231.15	102.61	40.713	261.83	83.14	40.374			
107.87	60.79	39.577	231.62	103.29	40.710	264.83	83.59	40.398	212.13	97.30	40.231
108.19	86.31	39.634	232.02	105.18	40.705	267.89	84.23	40.416	212.71	98.84	40.223
108.47	219.85	39.793	232.34	105.63	40.703	270.99	84.71	40.439	213.23	101.33	40.221
108.76	67.41	39.970	232.67	107.42	40.697	274.08	84.98	40.450	213.75	103.52	40.213
109.09	59.67	40.023	233.00	108.60	40.695	277.16	85.34	40.479	214.28	107.18	40.209
109.42	58.16	40.056	233.32	111.72	40.692	280.26	85.77	40.502	214.71	111.35	40.200
109.78	57.09	40.080				283.34	86.07	40.523	215.05	115.10	40.192
110.19	57.04	40.103	232.76	106.04	40.697	286.40	86.23	40.554	215.40	122.53	40.184
110.68	55.39	40.129	233.11	109.44	40.697	289.44	86.70	40.572	215.74	131.04	40.171
111.23	54.51	40.156	233.46	112.27	40.690	292.47	87.45	40.596	216.07	140.15	40.155
111.79	53.88	40.174	233.79	117.54	40.690	295.52	87.63	40.617	216.35	162.43	40.150
112.41	53.47	40.197	234.14	125.37	40.679	298.55	87.58	40.643	216.59	140.55	40.132
113.18	52.92	40.221	234.48	138.90	40.761	P = 108.0 MPa			216.83	130.30	40.119
114.16	52.53	40.247	234.79	146.24	40.671				217.15	113.52	40.116
115.35	52.28	40.281	235.10	128.80	40.661	107.56	46.96	38.985	217.47	102.13	40.111
116.64	52.20	40.307	235.40	112.34	40.658	110.56	47.57	39.014	217.82	93.73	40.111
117.93	52.12	40.330	235.72	101.36	40.653	112.60	48.37	39.040	218.19	88.76	40.114
119.52	52.29	40.359	236.03	95.69	40.645	115.03	49.25	39.064	218.56	85.69	40.119
121.58	52.66	40.380	236.35	91.52	40.645	117.53	50.21	39.095	219.01	82.98	40.114
124.23	53.33	40.398	236.67	87.70	40.645	119.98	51.17	39.118	219.54	81.23	40.109
127.06	53.95	40.419	236.99	84.51	40.645	122.44	51.95	39.139	220.07	80.20	40.109
128.14	54.31	40.419	237.32	84.60	40.648	124.95	52.82	39.160	220.60	77.97	40.109
130.58	54.91	40.432	237.64	83.55	40.645	127.44	53.59	39.181	221.13	78.53	40.103
132.98	56.03	40.445	237.98	83.52	40.645	129.95	54.42	39.197	222.46	78.44	40.119
135.51	56.19	40.458	238.43	82.48	40.651	132.54	55.30	39.217			
138.15	57.37	40.471	238.96	81.63	40.653	135.09	56.09	39.233	207.73	89.93	40.262
140.77	57.93	40.484	239.50	81.81	40.648	137.63	57.10	39.249	209.10	91.79	40.257
143.36	58.75	40.499	240.04	81.84	40.648	140.18	57.71	39.267	209.86	92.30	40.241
145.93	59.59	40.510	240.58	80.99	40.656	142.75	58.74	39.280	210.38	93.71	40.239
148.47	60.49	40.520	241.25	81.61	40.661	145.30	59.28	39.296	210.80	94.73	40.236
150.99	61.02	40.536	242.19	81.23	40.671	147.82	60.57	39.316	221.39	95.76	40.231
153.53	62.04	40.549	243.26	80.78	40.679	150.42	61.27	39.332	211.89	96.77	40.231
156.10	62.55	40.562	244.33	81.32	40.687	153.09	62.57	39.350	212.39	98.81	40.223
158.70	63.69	40.580				155.74	63.60	39.368	212.85	100.25	40.226
161.33	64.23	40.598	242.13	80.84	40.671	158.36	64.95	39.379	213.27	102.03	40.221
163.94	65.11	40.614	244.44	81.12	40.687	160.97	66.15	39.405	213.68	104.02	40.215
166.53	66.17	40.627	247.07	81.55	40.703	163.55	67.30	39.426	214.09	107.20	40.210
169.10	66.84	40.643	249.77	82.02	40.721	166.11	68.86	39.447	214.79	113.38	40.202
171.65	67.19	40.656	252.46	81.73	40.739	168.47	71.88	39.470	215.12	119.43	40.192
174.19	67.99	40.664	255.14	82.48	40.755	169.81	78.94	39.499	215.44	124.09	40.184
176.71	68.61	40.679	257.81	82.75	40.773	170.26	81.64	39.517	215.76	134.17	40.171
179.21	69.53	40.690	260.48	83.34	40.794	170.60	108.34	39.546	216.07	142.44	40.155
181.75	70.72	40.700	263.14	83.46	40.810	170.91	284.84	39.692	216.38	146.84	40.142
184.31	71.48	40.710	265.79	84.17	40.833	171.20	130.22	39.814	216.70	135.99	40.132
186.88	72.34	40.724	268.43	84.35	40.851	171.54	109.54	39.874	217.02	119.91	40.122
189.46	73.60	40.724	271.06	85.25	40.867	171.88	100.88	39.916	217.34	106.74	40.111
192.03	74.85	40.734	273.70	85.07	40.883	172.22	94.39	39.957	217.67	96.85	40.111
194.59	75.55	40.742	276.36	85.51	40.905	172.65	92.28	39.999	218.04	91.32	40.116
197.13	76.67	40.747	279.01	85.55	40.929	173.18	86.44	40.043	218.44	86.07	40.114
199.65	77.94	40.755	281.64	86.53	40.945	173.71	83.58	40.072	218.85	83.61	40.119
202.18	78.77	40.760	284.28	85.75	40.963	174.24	80.74	40.098	219.25	82.68	40.116
204.71	80.18	40.755				174.86	78.83	40.116	219.66	81.52	40.109
207.31	81.85	40.765	224.98	78.39	40.132	175.90	77.00	40.142	220.06	80.12	40.109
209.39	83.05	40.765	226.25	78.40	40.142	177.03	74.93	40.171	220.47	79.40	40.103
211.96	83.88	40.768	228.02	78.55	40.155	178.00	74.57	40.189	220.95	79.18	40.106
214.52	85.32	40.768	230.19	78.59	40.163	179.59	74.23	40.208	221.52	78.65	40.109

Agreement between the present and previous data is found also in the entropies of the transition as shown in Table 1.[10-12] The difference (up to 8%) would not be significant because the entropy values depend primarily upon choice of the baseline which one has to assume in the wide temperature range of occurrence of the phase transition.

Heat Capacities under Pressures. Figure 3 shows the results of molar heat capacity and molar volume of NH_4Br at 0.101 and 108.0 MPa. The numerical values are collected in Table 2. Application of the pressure increased the δ-γ phase transition temperature from 108.5 K to 170.9 K and decreased the γ-β one from 234.8 K to 216.4 K. The transition temperatures observed at 108.0 MPa are in good accordance with those on the phase diagram reported before.[13,14] The slope of the transition line, dT_{tr}/dp, is 0.578 K MPa^{-1} for the δ-γ phases and -0.171 K MPa^{-1} for the γ-β phases.

Figure 4 shows the molar heat capacity and molar volume of ND_4Br at 0.101, 50.0, and 111.0 MPa in the temperature range of 130 to 260 K. The numerical values are given in Table 3. The two phase transitions, δ-γ and γ-β, observed at 168.5 and 215.5 K at 0.101 MPa, got close in temperature to each other with the increasing pressure to take place at 194.3 and 206.0 K at 50.0 MPa, and coalesced into one, direct transformation from δ to β phases, around 67 MPa at 201.2 K. The transition temperature was 205.3 K at 111.0 MPa.

The δ-γ phase transition was accompanied with a large expansion in volume, and had a increasingly larger premonitory region on the low temperature side as the pressure was increased. The slope of the transition line, dT_{tr}/dp, was 0.517 K MPa^{-1}. The

TABLE 3. MOLAR HEAT CAPACITY AND MOLAR VOLUME OF ND_4Br

T/K	C_p/J K^{-1}mol^{-1}	V/cm^{3}mol^{-1}
P = 101 kPa		
128.60	60.35	39.351
131.64	61.40	39.400
134.64	61.43	39.426
137.60	63.52	39.440
140.71	64.21	39.460
143.96	65.51	39.469
147.17	66.74	39.498
150.40	67.92	39.506
153.58	69.51	39.503
156.77	70.69	39.521
159.92	72.78	39.549
162.01	73.73	39.567
162.87	74.80	39.572
163.55	75.41	39.578
164.11	75.87	39.584
164.52	76.07	39.584
164.93	76.81	39.584
165.34	77.07	39.587
165.75	77.41	39.584
166.16	78.67	39.584
166.57	79.22	39.584
166.98	80.08	39.587
167.39	80.52	39.601
167.79	85.44	39.598
168.55	261.97	39.739
168.89	192.52	39.898
169.25	119.13	39.995
169.64	108.68	40.047
170.03	103.32	40.099
170.42	95.55	40.131
170.82	94.50	40.145
171.22	90.74	40.171
171.62	88.37	40.191
172.31	85.83	40.217
173.31	83.39	40.249
174.48	81.15	40.286
175.81	79192	40.301
177.48	78.94	40.318
180.46	78.82	40.326
184.40	79.99	40.344
188.32	81.57	40.358
192.20	83.26	40.361
196.04	85.32	40.355
199.80	88.33	40.358
203.18	90.41	40.370
205.75	93.05	40.358
207.99	95.95	40.347
209.27	98.05	40.349
209.80	98.60	40.352
210.22	99.91	40.347
210.64	100.53	40.347
211.06	101.87	40.347
211.48	102.98	40.341
211.90	104.30	40.326
212.32	106.51	40.324
212.73	108.56	40.318
213.15	110.87	40.309
213.56	114.91	40.303
213.97	118.84	40.298
214.38	124.95	40.289
214.78	134.91	40.289
215.18	142.76	40.254
215.58	143.05	40.240
215.99	130.35	40.226
216.39	113.95	40.217
216.80	105.09	40.208
217.22	97.56	40.208
217.65	92.08	40.203
218.07	90.84	40.214
218.49	87.92	40.223
218.91	86.42	40.226
219.34	84.71	40.229
219.87	84.71	40.220
220.51	82.49	40.226
221.46	83.81	40.223
223.68	82.85	40.240
226.91	82.77	40.277
230.06	83.26	40.298
233.49	83.78	40.324
237.24	84.39	40.358
240.96	85.16	40.387
244.66	86.94	40.410
248.34	86.90	40.433
252.00	86.27	40.483
255.65	87.73	40.522
259.29	88.18	40.562
P = 50.0 MPa		
144.70	65.42	39.236
147.73	66.36	39.285
150.74	67.17	39.325
153.89	68.81	39.365
157.39	69.96	39.411
161.02	71.51	39.434
164.61	73.39	39.454
168.16	74.96	39.479
171.16	76.69	39.512
175.16	79.17	39.555
178.61	81.25	39.558
181.68	84.06	39.590
184.07	85.68	39.607
186.09	88.43	39.630
187.43	90.85	39.647
188.09	91.47	39.650
188.76	92.28	39.656
189.42	93.14	39.664
190.08	94.42	39.664
190.74	96.29	39.670
191.29	96.87	39.687
191.72	100.01	39.711
192.16	100.16	39.742
192.59	102.34	39.762
193.45	108.86	39.806
193.88	131.08	39.834
194.26	290.67	39.972
194.62	131.04	40.119
195.02	114.66	40.165
195.45	104.59	40.194
195.88	103.65	40.208
196.42	99.60	40.229
197.07	97.25	40.246
197.72	95.79	40.260
198.37	95.05	40.272
199.18	95.64	40.278
200.15	96.65	40.272
201.12	100.42	40.269
201.82	98.59	40.269
202.25	99.35	40.269
202.68	101.71	40.275
203.10	102.97	40.272
203.53	106.51	40.266
203.95	109.43	40.260
204.37	114.75	40.246
204.79	123.13	40.231
205.20	139.27	40.211
205.59	189.80	40.185
205.97	226.21	40.142
206.35	136.07	40.105
206.77	106.11	40.082
207.30	92.88	40.076
207.94	86.99	40.076
208.59	83.87	40.082
209.24	82.81	40.093
209.89	81.59	40.102
210.87	81.54	40.102
212.82	81.28	40.122
215.72	81.20	40.139
218.94	81.13	40.157
222.15	81.50	40.180
224.91	81.46	40.188
228.08	82.17	40.211
231.56	82.46	40.231
235.33	83.43	40.249
239.09	84.89	40.266
242.83	84.90	40.289
246.54	85.50	40.315
249.01	85.89	40.329
P = 57.0 MPa		
155.58	69.49	39.264
158.47	72.58	39.351
162.05	72.25	39.411
165.59	73.94	39.457
169.09	75.02	39.486
172.56	77.11	39.512
175.99	79.37	39.538
179.39	81.61	39.558
182.75	84.99	39.587
186.07	87.94	39.601
188.25	91.12	39.604
189.23	92.33	39.598
190.21	94.40	39.607
191.02	95.89	39.618
191.68	97.45	39.630
192.33	98.57	39.641
192.99	100.08	39.659
193.64	101.87	39.672
194.29	103.97	39.682
194.94	106.28	39.696
195.59	109.27	39.705
196.23	113.17	39.722
196.74	117.09	39.736
197.12	125.02	39.811
197.49	160.87	39.846
197.84	249.85	39.964
198.19	117.54	40.076
198.57	111.94	40.108
198.95	109.03	40.131
199.34	104.16	40.154
199.73	104.13	40.162
200.11	105.78	40.177
200.50	107.25	40.185
200.88	114.12	40.183
201.26	111.96	40.191
201.65	103.43	40.191
202.03	103.38	40.180
202.42	105.75	40.171
202.80	109.79	40.165
203.18	115.64	40.157
203.56	124.97	40.148
203.93	143.52	40.139
204.28	192.82	40.119
204.62	245.77	40.070
204.97	134.18	40.030
205.34	103.26	40.014
205.73	93.60	40.007
206.25	87.89	40.010
206.90	84.83	40.018
207.55	83.28	40.027
208.21	81.85	40.027
208.86	81.20	40.030
209.85	81.32	40.033
213.00	80.77	40.067
216.14	80.66	40.076
218.41	81.01	40.079
221.64	81.68	40.171
224.85	81.86	40.183
228.04	82.61	40.237
231.22	82.51	40.237
228.34	82.40	40.099
231.47	82.69	40.183
234.58	83.19	40.183
237.98	84.00	40.209
241.68	84.53	40.226
245.36	85.63	40.240
249.04	86.53	40.257
252.68	85.30	40.275
P = 62.0 MPa		
162.70	71.47	39.285
166.30	73.41	39.285
169.85	75.37	39.411
173.37	75.95	39.475
176.86	79.61	39.515
180.31	82.38	39.546
183.72	85.38	39.578
187.10	89.75	39.595
190.44	94.04	39.650
193.73	100.68	39.693
196.02	108.33	39.722
196.99	112.52	39.731
197.63	117.65	39.745
198.26	122.76	39.762
198.76	129.53	39.780
199.13	135.64	93.791
199.50	156.06	39.803
199.86	175.84	39.849
200.21	187.74	39.964
200.57	138.64	40.062
200.93	173.72	40.093
201.29	134.52	40.111
201.67	106.34	40.113
202.06	107.38	40.111
202.44	116.83	40.099
202.81	127.92	40.093
203.18	156.36	40.076
203.53	227.73	40.044
203.87	162.97	40.018
204.24	114.37	40.001
204.75	87.78	39.998
205.41	86.33	39.998
206.06	82.95	40.004
206.72	82.83	40.013
207.37	80.79	40.010
208.69	80.62	39.995
211.30	80.66	40.007
212.15	80.22	39.961
214.92	80.66	40.001
217.83	80.63	40.042
220.90	80.64	40.073
224.11	81.60	40.088
227.31	81.82	40.111
230.49	82.51	40.122
233.66	82.75	40.145
236.82	83.66	40.168
P = 63.5 MPa		
161.35	71.89	39.340
164.96	73.41	39.394
168.54	75.24	39.460
172.07	76.91	39.518
175.57	79.06	39.552
179.03	81.14	39.576
182.46	84.49	39.610
185.84	87.16	39.652
189.19	91.77	39.684
191.48	95.75	39.741
192.86	98.31	39.738
194.17	101.90	39.755
195.47	105.09	39.773
196.76	111.65	39.791
197.72	116.86	39.809
198.35	122.25	39.822
198.85	127.15	39.835
199.23	133.63	39.842
199.60	141.24	39.854
199.96	154.55	39.866
200.32	180.35	39.882
200.66	251.18	40.010
201.00	152.92	40.134
201.37	139.36	40.142
201.74	110.56	40.141
202.12	116.94	40.123
202.86	171.52	40.107
203.21	203.17	40.082
203.56	135.27	40.052
203.94	104.81	40.040
204.33	95.10	40.043
204.85	89.60	40.048
205.50	85.87	40.048
206.16	83.41	40.049
206.98	82.41	40.050
207.96	81.34	40.047
210.09	80.88	40.049
213.35	80.77	40.070
214.58	80.76	40.069
217.82	81.04	40.069
221.05	81.25	40.083
224.26	81.70	40.100
P = 65.0 MPa		
162.38	72.09	39.304
165.98	73.56	39.384
169.54	75.13	39.453
173.08	77.68	39.522
176.57	79.71	39.554
180.02	82.05	39.580
183.43	85.08	39.609
186.81	88.09	39.646
190.15	93.01	39.672
192.47	97.69	39.701
193.81	100.70	39.733
195.11	104.31	39.741
196.40	108.70	39.756
197.68	115.89	39.773
198.50	120.88	39.790
198.88	127.71	39.802
199.26	132.76	39.813
199.63	138.86	39.831
199.99	150.71	39.842
200.35	168.60	39.859
200.70	221.42	39.879
201.03	236.99	40.021
201.39	116.10	40.139
201.76	124.70	40.121
202.13	153.61	40.110
202.48	225.24	40.084
202.82	168.74	40.035
203.19	118.47	40.015
203.57	102.19	40.012
203.96	95.34	40.018
204.35	89.97	40.021
205.03	87.33	40.018
206.01	84.09	40.023
207.00	82.72	40.029
207.98	81.98	40.029
210.10	80.81	40.041
213.36	80.57	40.058
216.61	80.94	40.055
219.85	81.24	40.069
223.06	81.57	40.090
226.26	82.15	40.118
P = 66.0 MPa		
164.76	72.91	39.309
168.33	74.67	39.387
171.86	76.65	39.462
175.36	78.87	39.505
178.99	81.40	39.546
182.60	84.22	39.592
185.98	87.36	39.603
189.33	91.91	39.632
191.98	96.19	39.666
193.65	99.38	39.687
194.95	103.18	39.704
196.24	107.66	39.721
197.53	114.68	39.741
198.48	121.62	39.756
198.98	126.98	39.767
199.36	129.44	39.784
199.73	141.02	39.799
200.09	151.81	39.816

TABLE 3. (Continued)

T / K	C_p / J K^{-1}mol^{-1}	V / cm^{3}mol^{-1}	T / K	C_p / J K^{-1}mol^{-1}	V / cm^{3}mol^{-1}	T / K	C_p / J K^{-1}mol^{-1}	V / cm^{3}mol^{-1}	T / K	C_p / J K^{-1}mol^{-1}	V / cm^{3}mol^{-1}
200.45	170.53	39.831	200.61	174.75	39.816	170.39	74.96	39.264	226.98	82.58	39.958
200.80	230.09	39.856	200.96	229.75	39.833	173.17	76.99	39.282	229.96	82.91	39.978
201.08	709.14	39.954	201.22	887.67	39.868	175.94	78.79	39.313	232.98	83.25	39.967
201.38	122.11	40.009	201.43	246.06	39.911	178.68	79.98	39.336	237.30	84.18	39.986
201.76	114.71	40.012	201.83	96.62	39.940	181.84	82.89	39.400	241.66	84.94	40.065
202.14	124.76	40.003	202.22	90.07	39.951	184.55	84.55	39.431	244.99	85.78	40.099
202.51	112.86	39.997	202.75	86.58	39.954	187.21	86.66	39.457	248.30	86.56	40.128
202.90	102.91	39.995	203.40	84.21	39.966	189.86	89.19	39.474	251.35	86.79	40.134
203.28	96.70	39.889	204.06	82.94	39.969	192.43	93.25	39.500	254.49	86.94	40.168
203.97	92.11	39.889	204.88	82.03	39.974	195.08	96.28	39.529	257.67	87.75	40.185
204.94	87.27	39.986	206.03	81.19	39.972	197.66	103.62	39.609	260.86	88.39	40.240
205.92	84.71	39.983	208.33	80.32	40.012	199.20	109.27	39.584	264.09	88.18	40.272
206.90	83.41	39.980	211.60	80.31	40.023	199.67	112.56	39.590			
208.37	82.29	39.986	214.87	81.22	40.058	200.09	113.21	39.601	191.95	92.12	39.506
210.99	80.98	40.003	218.11	80.86	40.075	200.51	116.70	39.607	193.62	94.21	39.523
214.24	80.76	40.021	215.77	80.76	40.021	200.92	120.07	39.613	194.95	97.00	39.541
216.63	80.72	40.052	219.00	81.23	40.055	201.34	118.28	39.624	196.05	98.80	39.552
219.86	81.10	40.067	222.22	81.47	40.090	201.75	122.66	39.633	197.04	101.55	39.564
223.07	81.36	40.078	225.43	81.67	40.116	202.16	125.71	39.636	197.81	103.36	39.572
			228.62	81.97	40.136	202.58	123.97	39.641	198.24	103.39	39.578
P = 67.0 MPa			231.80	83.12	40.164	202.99	131.93	39.653	198.68	106.44	39.584
159.36	71.18	39.309	234.96	83.37	40.190	203.39	139.07	39.662	199.11	107.49	39.587
162.63	72.10	39.361				203.79	149.90	39.676	199.58	109.39	39.592
166.22	73.82	39.407	P = 111.0 MPa			204.19	161.72	39.693	199.97	110.80	39.598
169.78	75.15	39.451	121.76	58.12	38.861	204.57	192.62	39.708	200.40	112.58	39.607
173.30	77.58	39.497	124.34	58.54	38.913	204.93	271.95	39.731	200.83	115.98	39.616
176.78	79.42	39.517	126.91	59.53	38.962	205.25	485.14	39.762	201.26	117.48	39.624
180.23	80.07	39.552	129.43	60.29	38.944	205.59	127.47	39.808	201.68	121.34	39.630
183.65	85.30	39.589	131.99	61.38	39.014	206.01	95.34	39.808	202.11	123.84	39.636
187.02	88.43	39.612	134.58	61.87	39.046	206.44	88.87	39.805	202.53	128.06	39.639
189.70	92.25	39.620	137.15	62.62	39.072	206.87	86.20	39.817	202.95	132.53	39.650
191.69	95.86	39.643	139.70	63.86	39.086	207.30	84.89	39.817	203.36	141.11	39.662
193.66	99.31	39.672	142.22	64.66	39.109	207.73	82.64	39.826	203.77	150.51	39.679
195.63	104.68	39.695	144.74	65.35	39.123	208.16	84.08	39.828	204.18	165.87	39.693
197.09	111.13	39.721	147.46	66.54	39.146	208.59	82.95	39.834	204.57	194.38	39.708
197.88	116.06	39.733	150.39	67.10	39.155	209.22	82.60	39.841	204.94	291.32	39.722
198.39	119.08	39.741	153.30	67.77	39.161	210.53	78.77	39.846	205.26	467.34	39.762
198.77	124.50	39.759	156.19	69.10	39.169	213.11	81.14	39.849	205.62	120.77	39.808
199.15	127.87	39.764	159.04	70.61	39.184	215.68	81.42	39.866	206.05	92.40	39.811
199.52	132.15	39.781	161.90	71.40	39.195	218.29	81.96	39.889	206.49	87.28	39.817
199.89	141.28	39.793	164.75	72.82	39.215	221.09	81.75	39.903	206.93	86.64	39.823
200.26	153.15	39.805	167.58	74.08	39.214	224.04	82.21	39.935	207.37	84.10	39.826

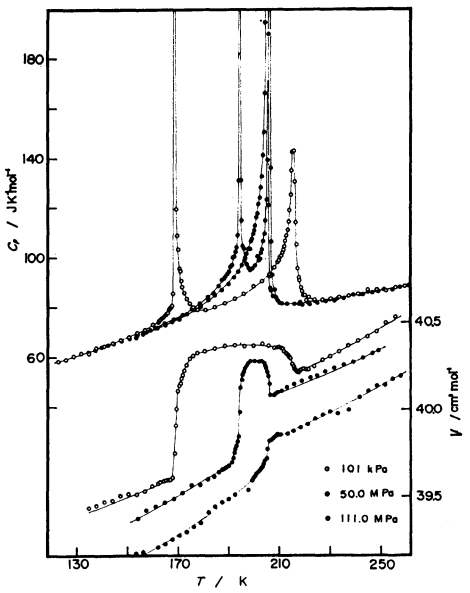

Fig. 4. Molar heat capacity and molar volume of ND_4Br at 0.101 (○), 50.0 (⊕), and 111.0 MPa (●).

γ-β transition, accompanied by the contraction of the volume, got sharper with the increasing pressure. The slope was given as -0.190 K MPa^{-1}. Both slopes of the transition lines changed slightly by deuteration. The deuteration has the same effect on the γ-β transition temperature as Br substitution has in the mixed crystal $NH_4Cl_xBr_{1-x}$.[15] The heat capacities of the β phase above *ca.* 220 K and the δ phase below *ca.* 150 K did not depend on the pressure. This is related to another experimental fact that the volume expansivity is independent of the temperature as required by the thermodynamic relation $(\partial C_P/\partial p)_T = -T(\partial^2 V/\partial T^2)_P$.

Figures 5(a)—(f) shows the temperature dependence of the molar heat capacity and molar volume at the constant pressures (given in the diagram) around the triple point. Those values are tabulated in Table 3. There was another heat capacity anomaly at 57.0 MPa and 62.0 MPa between the temperatures of two phase transitions described above, though the corresponding volume change was too small to be detected. As the pressure increased up to 63.1 MPa to 65.0 MPa, this anomaly overlapped with and merged into the δ-γ phase transition. At 66.0 MPa the heat capacity peak due to the γ-β transition at 202.1 K became quite small, indicating that a very small part of the crystal underwent the transition from the γ to β phases and that most from the δ to β phases. Heat capacity and volume curves at 67.0 MPa were essentially the same as those at 111.0 MPa.

The phase transition temperatures taken as the temperatures of the heat capacity peaks are plotted as a function of pressure as open circles in Fig. 6 where the dashed line stands for the result derived from a dilatometric study by Stevenson.[1] The present result indicates, in contrast to the previous one, that there is no maximum in any one branch of transition lines and the triple point is represented essentially as the point of intersection of the three straight lines. Absence of an exact triplet point in a very close look would be connected with a superheating effect in the δ-γ phase transition and will be discussed later.

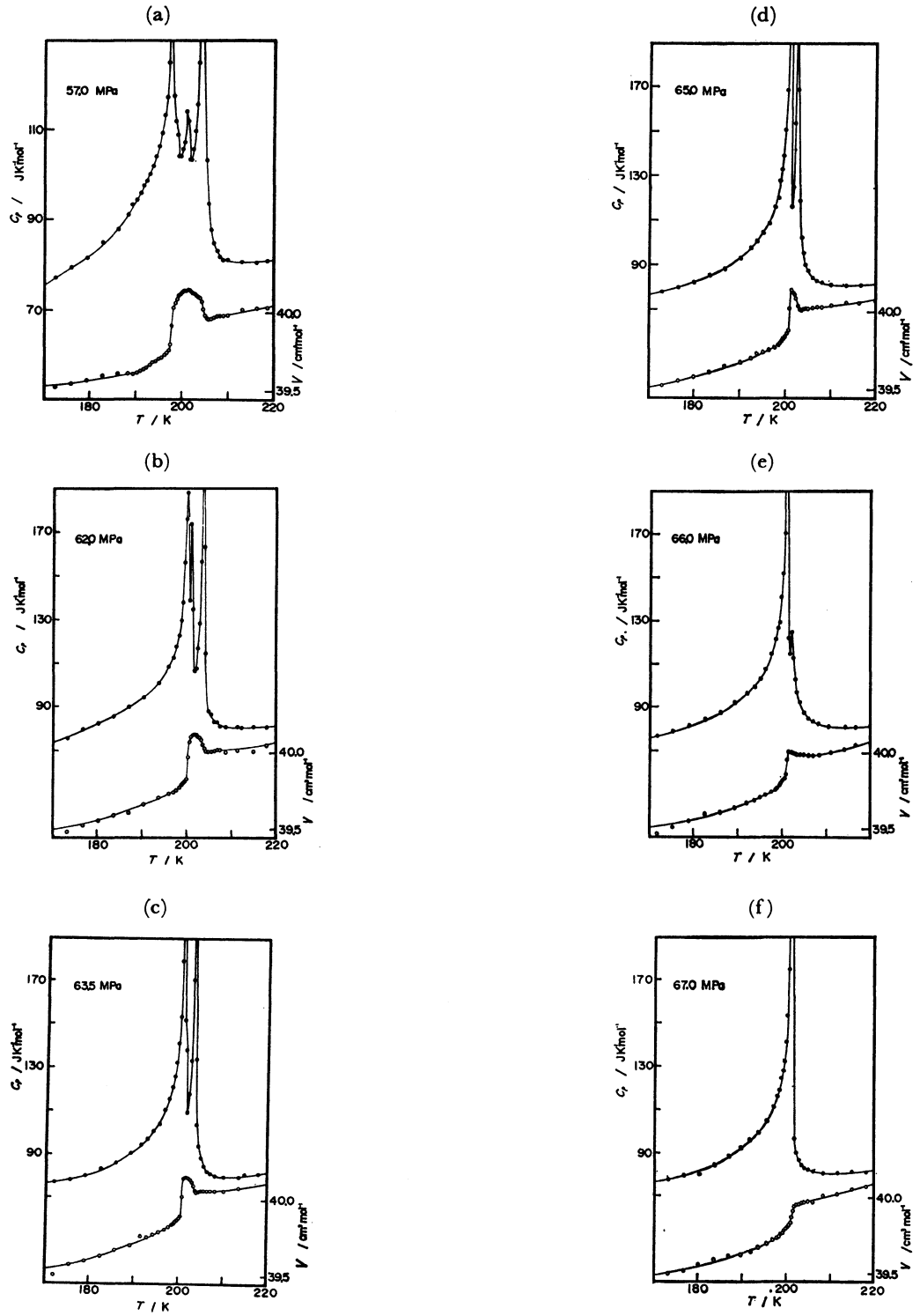

Fig. 5. Temperature dependences of molar heat capacity and molar volume of ND_4Br at the pressures around the triple point.
(a): 57.0 MPa, (b): 62.0 MPa, (c): 63.5 MPa, (d): 65.0 MPa, (e): 66.0 MPa, (f): 67.0 MPa.

Pressure Dependence of the Entropy of the Transition. The excess entropy involved in the successive two transitions for NH_4Br at 0.101 and 108.0 MPa are shown as functions of the temperature in Fig. 7. Here the entropy values were computed by assuming a baseline that joins smoothly the heat capacity curves outside the transition region. The total entropy change associated with the δ-γ-β phase transitions was estimated to be (4.0 ± 0.2) J K^{-1} mol^{-1}.

Figure 8 shows temperature dependence of the entropies of transition in ND_4Br at 0.1, 50.0, and 111.0 MPa and Fig. 9 at six pressures around the triple point. Table 4 lists the total entropy of transition from δ to β phases at all the pressures measured on ND_4Br. There

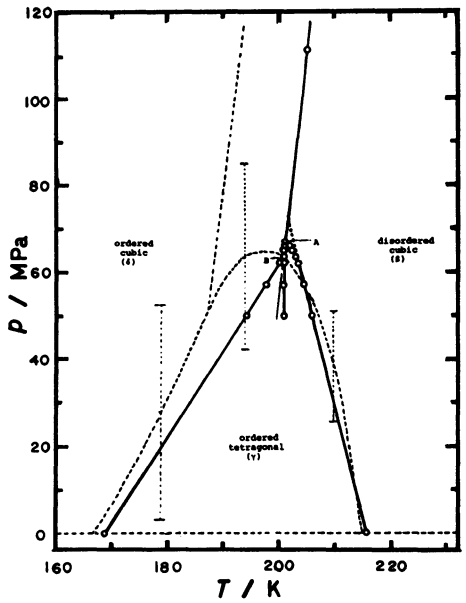

Fig. 6. Phase diagram of ND_4Br crystal as taken from the temperature of heat capacity peak. Previous data by R. Stevenson[1] are represented by dotted lines and error bars.

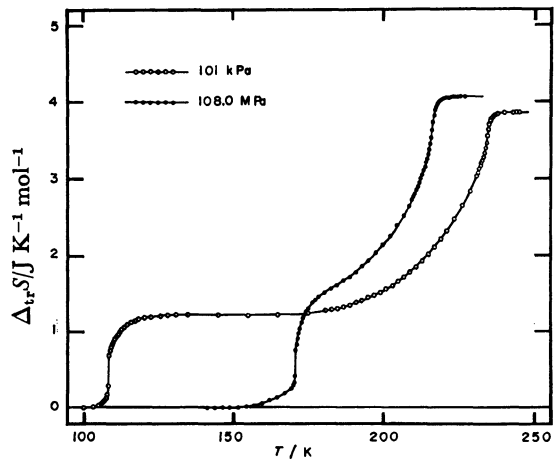

Fig. 7. Temperature dependence of the entropy of δ-γ-β phase transition in NH_4Br.
—○—: 0.101 MPa, —●—: 108.0 MPa.

is no pressure dependence in these values. The values can be explained in terms of the order-disorder mechanism in the orientational degree of freedom of NH_4^+ ions.

Molecular Excitation in the δ Phase. The entropies of transition had a very similar temperature dependence in the δ phase for the five isobaric measurements ranging from 57.0 to 67.0 MPa, as shown in Fig. 15. Correspondingly, the excess heat capacity (ΔC_p) *vs.* temperature curves in the relevant temperature and

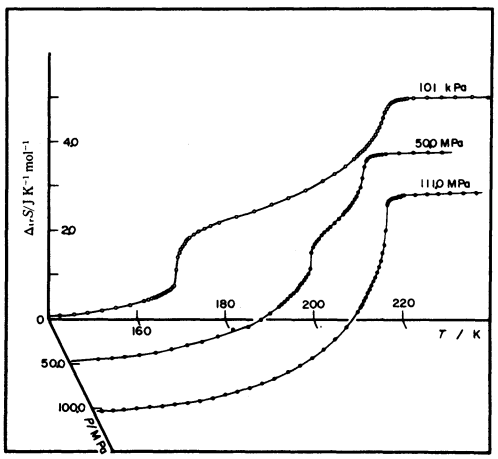

Fig. 8. Temperature dependence of the entropy of δ-γ-β phase transition in ND_4Br.
—○—: 0.101 MPa, —⊕—: 50.0 MPa, —●—: 110.1 MPa.

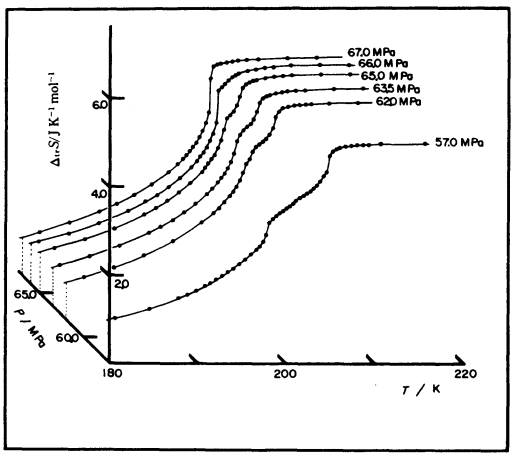

Fig. 9. Temperature dependence of the entropy of δ-γ-β phase transition in ND_4Br at six constant pressures around the triple point.

pressure region were practically independent of pressure as plotted in Fig. 10. It is to be noted here that the crystal transformed from the δ to γ phases below 66.0 MPa and from the δ to β phases at 67.0 MPa. These facts mean that the same process develops in the δ phase irrespective of the phases (γ or β) stable above the transition. This process is considered primarily to be the disordering of the orientation of NH_4^+ tetrahedra in the CsCl lattice, leading to the β phase. The δ-γ phase transition immediately below the triple point pressure therefore takes place between the cubic and tetragonal phases in the stages of low order parameters of the orientational arrangement of NH_4^+ ions.

Table 4. Pressure dependence of the entropy of δ-γ-β phase transition in ND_4Br crystal

P / MPa	0.101	50.0	57.0	62.0	63.5	65.0	66.0	67.0	111.0
$\Delta_\delta^\beta S$ / J K^{-1} mol^{-1}	5.00	4.87	4.94	4.86	4.88	4.91	5.00	4.88	4.96

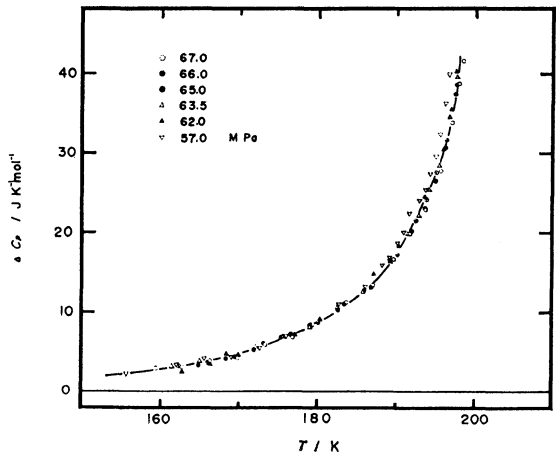

Fig. 10. Pressure and temperature dependences of the excess heat capacity due to the δ-γ or δ-β phase transition in ND_4Br crystal at around the triple point pressure.

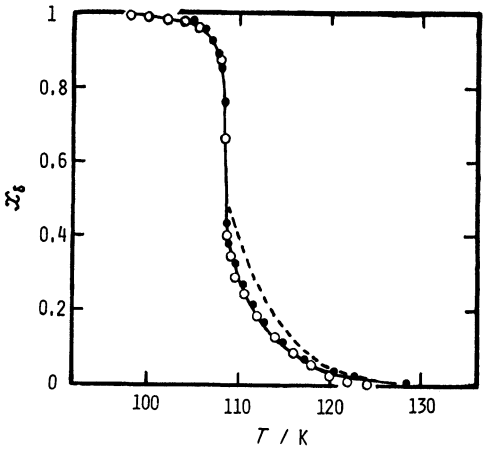

Fig. 11. Mole fraction of δ phase *vs.* temperature relation in the δ-γ phase transition of NH_4Br crystal at an atmospheric pressure.
—○—: Derived from the data of entropy, —●—: from the data of volume, ------: calculated by use of the Eq. 2.

Discussion on the Coexistence of the γ and δ Phases Domains. The δ-γ phase transition is of the first-order in which the entropy and volume undergo discontinuous change at the transition temperature. This is quite reasonable in view of the fact that the transition occurs between the parallel ordered cubic and the anti-parallel ordered tetragonal phases and that it can not proceed continuously as the homogeneous transition from one phase to the other from the viewpoint of crystal symmetry.

The heat capacity curve at 0.101 MPa in Fig. 1, however, shows a large post-transitional effect. The appearance of such an anomaly in a first-order transition as in the present case can be attributed to the coexistence of the domains of the δ and γ phases around the transition point. Actually the temperature dependence of the molar fraction of the δ phase calculated from the changes in entropy and volume associated with the transition can be explained by the spatial fluctuation of the domains as follows.[16-18]

Let x be the molar fraction of the δ phase, N the number of domains whose size is assumed to be the same throughout the crystal and G_δ and G_γ the free energies of the bulk δ and γ phases, respectively. Then the free energy of the crystal is, disregarding their interfacial energies, expressed by

$$G = [(1-x)G_\gamma + xG_\delta] + NkT[x \ln x + (1-x) \ln (1-x)]. \quad (1)$$

Minimization of the free energy at constant N and T gives the molar fraction

$$x = \frac{\exp\{-(G_\delta - G_\gamma)/NkT\}}{\exp\{-(G_\delta - G_\gamma)/NkT\}+1}. \quad (2)$$

Using the experimental values of 1.22 J K^{-1} mol^{-1} for the total entropy of transition and 108.5 K for the transition temperature in NH_4Br at 0.101 MPa, $(G_\delta - G_\gamma)$ can be approximated by the form 1.22 $(T/K - 108.5)$ J mol^{-1}. If one assumes that a single domain contains 6^3 (=216) NH_4^+ ions, the temperature dependence of the molar fraction x could be calculated as drawn with a broken line in Fig. 11.

Comparison of the calculated and the experimental values shows that the heat capacity anomaly described above is reproduced by this model of spatial fluctuation of δ and γ phases domains. The number of domains in the δ phase actually changes depending on the temperature and the pre-history of the sample, and the interfacial energy should be represented in the expression for the sample free energy. This will be discussed in the subsequent paper.

Superheating of the δ-γ Phase Transition. Superheating is possible in principle in the first-order phase transition, though not found frequently in contrast to supercooling. An evidence for the superheating in the δ-γ phase transition could be given by the consideration of the Gibbs free energies for the δ and γ phases. By way of an example the following discussion is established by the use of the calorimetric data at 50 MPa for ND_4Br. The free energies for the δ and γ phases on the basis of that for the β phase would be written down according to the Landau theory of phase transitions of the second kind as follows;

$$G(\eta^2) = G_\beta + \frac{a}{2}(T - T_0)\eta^2 + \frac{b}{4}\eta^4 + \frac{c}{6}\eta^6, \quad (3)$$

and

$$G(\xi^2) = G_\beta + \frac{a'}{2}(T - T_0')\xi^2 + \frac{b'}{4}\xi^4 + \frac{c'}{6}\xi^6, \quad (4)$$

where η and ξ are the order parameters describing the δ-β and the γ-β phase transitions, respectively, and G_β the free energy for the β phase. With coefficients a, b, c, T_0, a', b', c', and T_0' determined appropriately, the problems of which phase is stable at a given T and where the δ-γ phase transition takes place can be solved by the comparison between $G(\eta^2)$ and $G(\xi^2)$.

The coefficients a, b, c, and T_0 were derived by the extrapolation from those at 111.0 and 67.0 MPa at which the δ phase transformed directly into the β phase. The coefficients at the both pressures, 111.0 and 67.0 MPa, were obtained by use of the two equations;

$$\Delta_{tr}S(T) = S_0 - \frac{a}{2}\eta^2, \quad (5)$$

and

$$a(T-T_0) + b\eta^2 + c\eta^4 = 0, \quad (6)$$

where S_0 is the total entropy of the transition. The relation (5) connected with the experimental data of excess heat capacities yielded the temperature dependence of the order parameter, and the least-squares fit of the relation (6) to the T dependence of η^2 determined the coefficients at the respective pressure values. The coefficient values a', b', c', and T_0' were derived, using relations similar to Eqs. 5 and 6 with the order parameter ξ^2, from the experimental data at 50.0 MPa of the excess heat capacities associated with the γ-β phase transition.

Figure 12 shows the temperature dependence of the order parameters η^2 and ξ^2 with the coefficients thus determined. The δ-γ phase transition at 50.0 MPa took place at 194.3 K on heating in the actual experiment. The Gibbs energy against order parameter curves for both the δ and γ phases at the temperature and the pressure 50.0 MPa are shown in Fig. 13. The minimum free energy for the γ phase is definitely lower than that for the δ, contrary to the thermodynamic relation that the minimum values of free energies for the two phases should be equal to each other at the transition point. This means that the temperature of the heat capacity peak observed at 50.0 MPa is higher than the phase transition point as defined by the equality of the Gibbs energies; in other words, the substance in the δ phase at 194.3 K is in a superheated state.

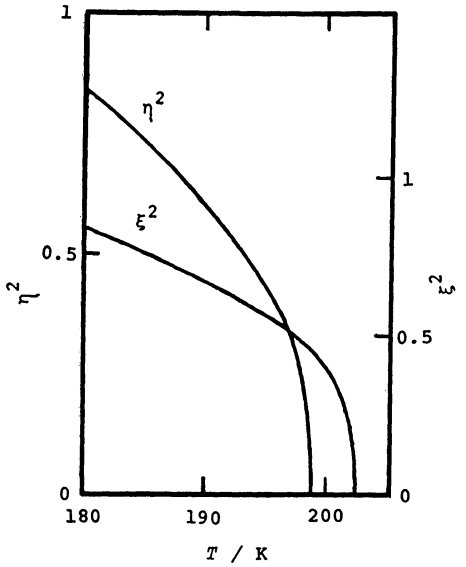

Fig. 12. Temperature dependences of the order parameters for γ and δ phases of ND_4Br at 50 MPa. The order parameter ξ is associated with the γ-β phase transition and η with the δ-β phase transition.

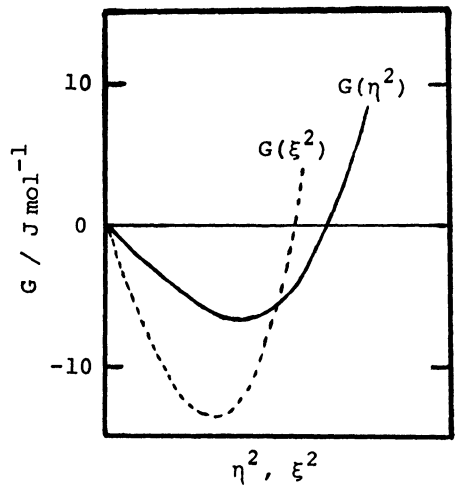

Fig. 13. Gibbs free energy against order parameter curves for the γ and δ phases at 194.3 K and 50 MPa. 194.3 K is the observed δ to γ phase transition point taken as the temperature of heat capacity peak 50.0 MPa.

Interpretation of an Anomalous Heat-capacity Peak. The phase diagram for ND_4Br (Fig. 6) has two peculiarities around the triple point among β, γ, and δ phases; one is the appearance of a new heat-capacity anomaly between the δ-γ and the γ-β phase transitions at pressures just below the triple point pressure, and the other is the apparent presence of two triple-points as shown by A and B. In this section the former phenomenon is discussed as the δ-β phase transition due to the coexistence of the δ and γ domains and of the superheating in the δ to γ phase change, the effects described above.

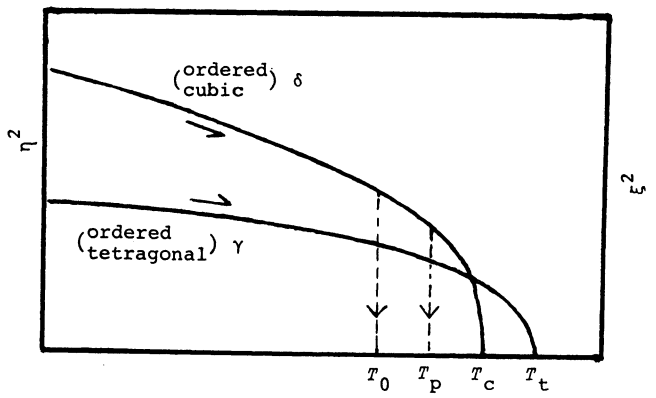

Fig. 14. Schematic temperature dependences of the order parameters for the δ-β and γ-β phase transitions in ND_4Br crystal at a certain constant pressure immediately below the triple point. T_0: the temperature at which $G_\delta = G_\gamma$, T_p: the δ-γ phase transition temperature, T_c: the δ-β phase transition temperature, T_t: the γ-β phase transition temperature.

Figure 14 illustrates diagramatically the path of transformation on heating as curves of order parameter versus temperature, where T_0 is the temperature of equilibrium between the δ and γ phases at which the free energies for the two phases become equal, and T_c and T_t are the temperatures of the δ-β and the γ-β phase changes, respectively. Most of domains of the δ phase transform into the γ phase around T_p with the superheating effect as indicated by an arrows, and subsequently into the β phase at T_t. But some of domains remain in the δ phase until the temperature T_c is reached, at which temperature they transform into the β phase directly. This fluctuational δ-β transition should become important as the pressure approaches

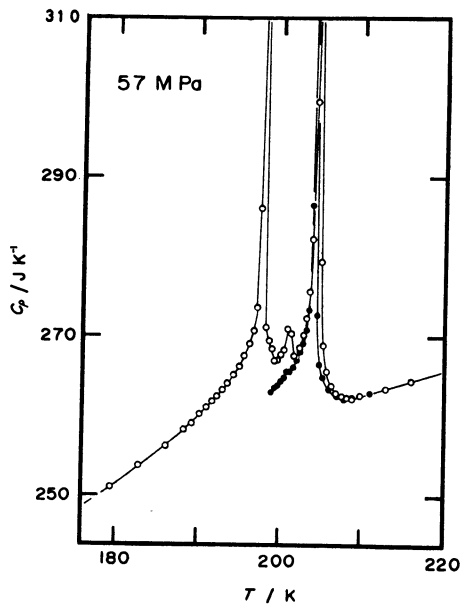

Fig. 15. The effect of thermal hysteresis on the heat capacity curve of ND_4Br crystal at 57.0 MPa. One series of measurement (—○—) was started at 100 K where the crystal was in the δ phase, and the other (—●—) was started at 198 K on the crystal in the γ phase after the treatment of the isothermal pressure increase from 0.101 to 57.0 MPa following the temperature decrease from room temperature to 198 K at 0.101 MPa.

that of the triple point, as the fraction of the substance, namely the number of domains, remaining in the δ phase accordingly increases till T_c.

Figure 15 shows another experimental evidence for the above reasoning with the use of heat capacity curves at 57 MPa as an example, the heat capacity values being the total of contributions from the sample and cell measured in the heating direction. Two sets of data, distinguished by open and solid circles, differed from each other in the prehistories of the sample. The sample in the former case (open circles) was cooled down to liquid nitrogen temperature so as to start the measurement in the δ phase. In the latter, on the other hand, the temperature of the samples was first decreased from 300 K to 198 K at an atmospheric pressure, then the pressure was isothermally increased to 57.0 MPa, and then a set of measurement was started from there in the heating direction. The former sample at 199.5 K, being normally in the γ phase, would consequently still have involved some domains of the δ phase resulting in the anomalous peak at 200.9 K on the subsequent heating while the latter would have been composed of the γ phase and if any the β phase. The results combined with the different thermal-prehistories of the sample therefore indicates the effects of superheating and coexistence as causing the anomalous heat-capacity peak in the decisive way.

It should be pointed out that the extra heat capacity peaks occur practically at the same temperature 200.8—200.9 K even though one would expect the peak temperature to follow the extrapolation of the stable δ-β phase boundary. This cannot be explained by the simplified domain model as discussed above. One would have to incorporate the possibility of distributed internal pressure felt by the less compact γ domains surrounded by the δ or β domains. The situation is, however, not clear at present.

Character of the γ-β Phase Transition around the Triple Point. As already pointed out there appeared two triple points, A and B in Fig. 6, on the phase diagram. The superheating of the δ-γ phase transition explains this unusual behavior of the phase lines (apart from the curvature of the γ-β line) in the close vicinity of the triple point. As we discussed above, the observed δ-γ phase boundary is at higher temperature than the equilibrium phase boundary by several Kelvin. The equilibrium δ-γ phase line which is assumed to be parallel to the observed phase line would then join the point A where the δ-β and γ-β phase boundaries meet thus terminating at a genuine triple point.

The γ-β phase line near the triple point A was found to deviate from a straight line (broken one in Fig. 6). This appears to be an equilibrium properties rather than a hysteretic effect related to the coexistence of the different domains, since the heat capacity measurement performed after approaching the triple point from the lower pressure gave essentially the same γ-β transition temperature. (See Fig. 15) The γ-β phase line is so curved that the β phase region is larger than the linear extrapolation of the γ-β phase line gives. This is explained if one notes that the two ionic interactions stabilizing the γ and δ phases are opposite in nature. The ionic interactions favoring the antiparallel orientation of the NH_4^+ ions within the ab plane stabilizes the γ phase and those favoring the parallel orientation the δ phase. The two interactions have the same strength in the opposite directions at the triple point. They tend to cancel each other resulting in relative stabilization of the disordered β phase, as is experimentally observed. Such fluctuational interaction among different phases does not occur at an ordinary triple point among a solid, liquid, and vapour. It is characteristic of a triple point involving phase transitions of the second kind.[19]

Concluding Remarks

The present results of heat capacity of NH_4Br and ND_4Br crystals evidenced again that the high pressure calorimeter described in the preceding paper has a satisfactory accuracy. The accurate measurements enabled the exact determination of p-T phase diagrams and the detailed examination of phase transitions to be performed under well specified thermodynamic conditions.

The peculiar phenomena observed at high pressures just below a triple point for ND_4Br crystal were reasonably explained in terms of the effects of superheating in the δ-γ phase transition and of coexistence of the δ, γ, and β phases domains (This is quite an instructive point in that the superheating effect causes a new phenomenon in some cases.). The nucleation and growth processes in the δ-γ phase transition is an interesting subject for

further study, as will be described in the subsequent paper. The detailed measurement of the δ-β phase transition line under high pressure (beyond the pressure range of the present apparatus) is desirable for the insight into the competitive interaction between the two different (parallel and anti-parallel) orderings in the disordered β phase.

References

1) R. Stevenson, *J. Chem. Phys.*, **34**, 1757 (1961).
2) C. W. Garland and R. A. Young, *J. Chem. Phys.*, **49**, 5282 (1968).
3) E. L. Wagner and D. F. Horning, *J. Chem. Phys.*, **18**, 305 (1950).
4) Y. Yamada, M. Mori, and Y. Noda, *J. Phys. Soc. Jpn.*, **32**, 1565 (1972).
5) M. Oguni, K. Watanabe, T. Matsuo, H. Suga, and S. Seki, *Bull. Chem. Soc. Jpn.*, **55**, 77 (1982).
6) C. W. Garland and C. F. Yarnell, *J. Chem. Phys.*, **44**, 1112 (1966).
7) R. S. Seymour, *Acta Crystallogr., Sect. A*, **27**, 348 (1971).
8) Y. Yamada, Y. Noda, J. D. Axe, and G. Shirane, *Phys. Rev. B*, **9**, 4429 (1974).
9) C. Rotter and W. Kamitakahara, *Phys. Rev. B*, **14**, 1983 (1976).
10) A. R. Cole, Doctoral Thesis, Massachusetts Institute of Technology, 1950.
11) M. Sorai, H. Suga, and S. Seki, *Bull. Chem. Soc. Jpn.*, **38**, 1125 (1956).
12) C. C. Stephenson and A. M. Karo, *J. Chem. Phys.*, **48**, 104 (1968).
13) W. Mandena and N. J. Trappeniers, *Physica*, **81B**, 285 (1976).
14) C. W. Garland, R. C. Leung, and F. P. Missel, *Phys. Rev. B*, **18**, 4848 (1978).
15) C. W. Garland, R. C. Leung, and C. Zahradnik, *J. Chem. Phys.*, **71**, 3158 (1979).
16) J. Frenkel, "Kinetic Theory of Liquids," Dover, New York (1955), p. 382.
17) A. R. Ubbelohde, "The Molten State of Matter," John Wiley and Sons, New York (1978), p. 86.
18) A. Kosaki, M. Sorai, H. Suga, and S. Seki, *Bull. Chem. Soc. Jpn.*, **50**, 810 (1977).
19) L. D. Landau and E. M. Lifshitz, "Statistical Physics," 3rd ed, Pergamon Press, Oxford (1980), Part 1, p. 497.